

Measurement of the effective weak mixing angle in $p\bar{p} \rightarrow Z/\gamma^* \rightarrow e^+e^-$ events

V.M. Abazov,³¹ B. Abbott,⁶⁷ B.S. Acharya,²⁵ M. Adams,⁴⁶ T. Adams,⁴⁴ J.P. Agnew,⁴¹ G.D. Alexeev,³¹ G. Alkhazov,³⁵ A. Alton^a,⁵⁶ A. Askew,⁴⁴ S. Atkins,⁵⁴ K. Augsten,⁷ C. Avila,⁵ F. Badaud,¹⁰ L. Bagby,⁴⁵ B. Baldin,⁴⁵ D.V. Bandurin,⁷³ S. Banerjee,²⁵ E. Barberis,⁵⁵ P. Baringer,⁵³ J.F. Bartlett,⁴⁵ U. Bassler,¹⁵ V. Bazterra,⁴⁶ A. Bean,⁵³ M. Begalli,² L. Bellantoni,⁴⁵ S.B. Beri,²³ G. Bernardi,¹⁴ R. Bernhard,¹⁹ I. Bertram,³⁹ M. Besançon,¹⁵ R. Beuselinck,⁴⁰ P.C. Bhat,⁴⁵ S. Bhatia,⁵⁸ V. Bhatnagar,²³ G. Blazey,⁴⁷ S. Blessing,⁴⁴ K. Bloom,⁵⁹ A. Boehnlein,⁴⁵ D. Boline,⁶⁴ E.E. Boos,³³ G. Borissov,³⁹ M. Borysova^l,³⁸ A. Brandt,⁷⁰ O. Brandt,²⁰ R. Brock,⁵⁷ A. Bross,⁴⁵ D. Brown,¹⁴ X.B. Bu,⁴⁵ M. Buehler,⁴⁵ V. Buescher,²¹ V. Bunichev,³³ S. Burdin^b,³⁹ C.P. Buszello,³⁷ E. Camacho-Pérez,²⁸ B.C.K. Casey,⁴⁵ H. Castilla-Valdez,²⁸ S. Caughron,⁵⁷ S. Chakrabarti,⁶⁴ K.M. Chan,⁵¹ A. Chandra,⁷² E. Chapon,¹⁵ G. Chen,⁵³ S.W. Cho,²⁷ S. Choi,²⁷ B. Choudhary,²⁴ S. Cihangir,⁴⁵ D. Claes,⁵⁹ J. Clutter,⁵³ M. Cooke^k,⁴⁵ W.E. Cooper,⁴⁵ M. Corcoran,⁷² F. Couderc,¹⁵ M.-C. Cousinou,¹² D. Cutts,⁶⁹ A. Das,⁴² G. Davies,⁴⁰ S.J. de Jong,^{29,30} E. De La Cruz-Burelo,²⁸ F. Déliot,¹⁵ R. Demina,⁶³ D. Denisov,⁴⁵ S.P. Denisov,³⁴ S. Desai,⁴⁵ C. Deterre^c,²⁰ K. DeVaughan,⁵⁹ H.T. Diehl,⁴⁵ M. Diesburg,⁴⁵ P.F. Ding,⁴¹ A. Dominguez,⁵⁹ A. Dubey,²⁴ L.V. Dudko,³³ A. Duperrin,¹² S. Dutt,²³ M. Eads,⁴⁷ D. Edmunds,⁵⁷ J. Ellison,⁴³ V.D. Elvira,⁴⁵ Y. Enari,¹⁴ H. Evans,⁴⁹ V.N. Evdokimov,³⁴ A. Fauré,¹⁵ L. Feng,⁴⁷ T. Ferbel,⁶³ F. Fiedler,²¹ F. Filthaut,^{29,30} W. Fisher,⁵⁷ H.E. Fisk,⁴⁵ M. Fortner,⁴⁷ H. Fox,³⁹ S. Fuess,⁴⁵ P.H. Garbincius,⁴⁵ A. Garcia-Bellido,⁶³ J.A. García-González,²⁸ V. Gavrilov,³² W. Geng,^{12,57} C.E. Gerber,⁴⁶ Y. Gershtein,⁶⁰ G. Ginther,^{45,63} O. Gogota,³⁸ G. Golovanov,³¹ P.D. Grannis,⁶⁴ S. Greder,¹⁶ H. Greenlee,⁴⁵ G. Grenier,¹⁷ Ph. Gris,¹⁰ J.-F. Grivaz,¹³ A. Grohsjean^c,¹⁵ S. Grünendahl,⁴⁵ M.W. Grünewald,²⁶ T. Guillemain,¹³ G. Gutierrez,⁴⁵ P. Gutierrez,⁶⁷ J. Haley,⁶⁸ L. Han,⁴ K. Harder,⁴¹ A. Harel,⁶³ J.M. Hauptman,⁵² J. Hays,⁴⁰ T. Head,⁴¹ T. Hebbeker,¹⁸ D. Hedin,⁴⁷ H. Hegab,⁶⁸ A.P. Heinson,⁴³ U. Heintz,⁶⁹ C. Hensel,¹ I. Heredia-De La Cruz^d,²⁸ K. Herner,⁴⁵ G. Hesketh^f,⁴¹ M.D. Hildreth,⁵¹ R. Hirosky,⁷³ T. Hoang,⁴⁴ J.D. Hobbs,⁶⁴ B. Hoeneisen,⁹ J. Hogan,⁷² M. Hohlfield,²¹ J.L. Holzbauer,⁵⁸ I. Howley,⁷⁰ Z. Hubacek,^{7,15} V. Hynek,⁷ I. Iashvili,⁶² Y. Ilchenko,⁷¹ R. Illingworth,⁴⁵ A.S. Ito,⁴⁵ S. Jabeen^m,⁴⁵ M. Jaffré,¹³ A. Jayasinghe,⁶⁷ M.S. Jeong,²⁷ R. Jesik,⁴⁰ P. Jiang,⁴ K. Johns,⁴² E. Johnson,⁵⁷ M. Johnson,⁴⁵ A. Jonckheere,⁴⁵ P. Jonsson,⁴⁰ J. Joshi,⁴³ A.W. Jung,⁴⁵ A. Juste,³⁶ E. Kajfasz,¹² D. Karmanov,³³ I. Katsanos,⁵⁹ M. Kaur,²³ R. Kehoe,⁷¹ S. Kermiche,¹² N. Khalatyan,⁴⁵ A. Khanov,⁶⁸ A. Kharchilava,⁶² Y.N. Kharzheev,³¹ I. Kiselevich,³² J.M. Kohli,²³ A.V. Kozelov,³⁴ J. Kraus,⁵⁸ A. Kumar,⁶² A. Kupco,⁸ T. Kurča,¹⁷ V.A. Kuzmin,³³ S. Lammers,⁴⁹ P. Lebrun,¹⁷ H.S. Lee,²⁷ S.W. Lee,⁵² W.M. Lee,⁴⁵ X. Lei,⁴² J. Lellouch,¹⁴ D. Li,¹⁴ H. Li,⁷³ L. Li,⁴³ Q.Z. Li,⁴⁵ J.K. Lim,²⁷ D. Lincoln,⁴⁵ J. Linnemann,⁵⁷ V.V. Lipaev,³⁴ R. Lipton,⁴⁵ H. Liu,⁷¹ Y. Liu,⁴ A. Lobodenko,³⁵ M. Lokajicek,⁸ R. Lopes de Sa,⁴⁵ R. Luna-Garcia^g,²⁸ A.L. Lyon,⁴⁵ A.K.A. Maciel,¹ R. Madar,¹⁹ R. Magaña-Villalba,²⁸ S. Malik,⁵⁹ V.L. Malyshev,³¹ J. Mansour,²⁰ J. Martínez-Ortega,²⁸ R. McCarthy,⁶⁴ C.L. McGivern,⁴¹ M.M. Meijer,^{29,30} A. Melnitchouk,⁴⁵ D. Menezes,⁴⁷ P.G. Mercadante,³ M. Merkin,³³ A. Meyer,¹⁸ J. Meyerⁱ,²⁰ F. Miconi,¹⁶ N.K. Mondal,²⁵ M. Mulhearn,⁷³ E. Nagy,¹² M. Narain,⁶⁹ R. Nayyar,⁴² H.A. Neal,⁵⁶ J.P. Negret,⁵ P. Neustroev,³⁵ H.T. Nguyen,⁷³ T. Nunnemann,²² J. Orduna,⁷² N. Osman,¹² J. Osta,⁵¹ A. Pal,⁷⁰ N. Parashar,⁵⁰ V. Parihar,⁶⁹ S.K. Park,²⁷ R. Partridge^e,⁶⁹ N. Parua,⁴⁹ A. Patwa^j,⁶⁵ B. Penning,⁴⁵ M. Perfilov,³³ Y. Peters,⁴¹ K. Petridis,⁴¹ G. Petrillo,⁶³ P. Pétrouff,¹³ M.-A. Pleier,⁶⁵ V.M. Podstavkov,⁴⁵ A.V. Popov,³⁴ M. Prewitt,⁷² D. Price,⁴¹ N. Prokopenko,³⁴ J. Qian,⁵⁶ A. Quadt,²⁰ B. Quinn,⁵⁸ P.N. Ratoff,³⁹ I. Razumov,³⁴ I. Ripp-Baudot,¹⁶ F. Rizatdinova,⁶⁸ M. Rominsky,⁴⁵ A. Ross,³⁹ C. Royon,¹⁵ P. Rubinov,⁴⁵ R. Ruchti,⁵¹ G. Sajot,¹¹ A. Sánchez-Hernández,²⁸ M.P. Sanders,²² A.S. Santos^h,¹ G. Savage,⁴⁵ M. Savitskiy,³⁸ L. Sawyer,⁵⁴ T. Scanlon,⁴⁰ R.D. Schamberger,⁶⁴ Y. Scheglov,³⁵ H. Schellman,⁴⁸ C. Schwanenberger,⁴¹ R. Schwienhorst,⁵⁷ J. Sekaric,⁵³ H. Severini,⁶⁷ E. Shabalina,²⁰ V. Shary,¹⁵ S. Shaw,⁴¹ A.A. Shchukin,³⁴ V. Simak,⁷ P. Skubic,⁶⁷ P. Slattery,⁶³ D. Smirnov,⁵¹ G.R. Snow,⁵⁹ J. Snow,⁶⁶ S. Snyder,⁶⁵ S. Söldner-Rembold,⁴¹ L. Sonnenschein,¹⁸ K. Soustruznik,⁶ J. Stark,¹¹ D.A. Stoyanova,³⁴ M. Strauss,⁶⁷ L. Suter,⁴¹ P. Svoisky,⁶⁷ M. Titov,¹⁵ V.V. Tokmenin,³¹ Y.-T. Tsai,⁶³ D. Tsybychev,⁶⁴ B. Tuchming,¹⁵ C. Tully,⁶¹ L. Uvarov,³⁵ S. Uvarov,³⁵ S. Uzunyan,⁴⁷ R. Van Kooten,⁴⁹ W.M. van Leeuwen,²⁹ N. Varelas,⁴⁶ E.W. Varnes,⁴² I.A. Vasilyev,³⁴ A.Y. Verkheev,³¹ L.S. Vertogradov,³¹ M. Verzocchi,⁴⁵ M. Vesterinen,⁴¹ D. Vilanova,¹⁵ P. Vokac,⁷ H.D. Wahl,⁴⁴ M.H.L.S. Wang,⁴⁵ J. Warchol,⁵¹ G. Watts,⁷⁴ M. Wayne,⁵¹ J. Weichert,²¹ L. Welty-Rieger,⁴⁸ M.R.J. Williamsⁿ,⁴⁹ G.W. Wilson,⁵³ M. Wobisch,⁵⁴ D.R. Wood,⁵⁵ T.R. Wyatt,⁴¹ Y. Xie,⁴⁵ R. Yamada,⁴⁵

S. Yang,⁴ T. Yasuda,⁴⁵ Y.A. Yatsunenko,³¹ W. Ye,⁶⁴ Z. Ye,⁴⁵ H. Yin,⁴⁵ K. Yip,⁶⁵ S.W. Youn,⁴⁵ J.M. Yu,⁵⁶
 J. Zennaro,⁶² T.G. Zhao,⁴¹ B. Zhou,⁵⁶ J. Zhu,⁵⁶ M. Zielinski,⁶³ D. Zieminska,⁴⁹ and L. Zivkovic¹⁴

(The D0 Collaboration*)

¹LAFEX, Centro Brasileiro de Pesquisas Físicas, Rio de Janeiro, Brazil

²Universidade do Estado do Rio de Janeiro, Rio de Janeiro, Brazil

³Universidade Federal do ABC, Santo André, Brazil

⁴University of Science and Technology of China, Hefei, People's Republic of China

⁵Universidad de los Andes, Bogotá, Colombia

⁶Charles University, Faculty of Mathematics and Physics,

Center for Particle Physics, Prague, Czech Republic

⁷Czech Technical University in Prague, Prague, Czech Republic

⁸Institute of Physics, Academy of Sciences of the Czech Republic, Prague, Czech Republic

⁹Universidad San Francisco de Quito, Quito, Ecuador

¹⁰LPC, Université Blaise Pascal, CNRS/IN2P3, Clermont, France

¹¹LPSC, Université Joseph Fourier Grenoble 1, CNRS/IN2P3,

Institut National Polytechnique de Grenoble, Grenoble, France

¹²CPPM, Aix-Marseille Université, CNRS/IN2P3, Marseille, France

¹³LAL, Université Paris-Sud, CNRS/IN2P3, Orsay, France

¹⁴LPNHE, Universités Paris VI and VII, CNRS/IN2P3, Paris, France

¹⁵CEA, Irfu, SPP, Saclay, France

¹⁶IPHC, Université de Strasbourg, CNRS/IN2P3, Strasbourg, France

¹⁷IPNL, Université Lyon 1, CNRS/IN2P3, Villeurbanne, France and Université de Lyon, Lyon, France

¹⁸III. Physikalisches Institut A, RWTH Aachen University, Aachen, Germany

¹⁹Physikalisches Institut, Universität Freiburg, Freiburg, Germany

²⁰II. Physikalisches Institut, Georg-August-Universität Göttingen, Göttingen, Germany

²¹Institut für Physik, Universität Mainz, Mainz, Germany

²²Ludwig-Maximilians-Universität München, München, Germany

²³Panjab University, Chandigarh, India

²⁴Delhi University, Delhi, India

²⁵Tata Institute of Fundamental Research, Mumbai, India

²⁶University College Dublin, Dublin, Ireland

²⁷Korea Detector Laboratory, Korea University, Seoul, Korea

²⁸CINVESTAV, Mexico City, Mexico

²⁹Nikhef, Science Park, Amsterdam, the Netherlands

³⁰Radboud University Nijmegen, Nijmegen, the Netherlands

³¹Joint Institute for Nuclear Research, Dubna, Russia

³²Institute for Theoretical and Experimental Physics, Moscow, Russia

³³Moscow State University, Moscow, Russia

³⁴Institute for High Energy Physics, Protvino, Russia

³⁵Petersburg Nuclear Physics Institute, St. Petersburg, Russia

³⁶Institució Catalana de Recerca i Estudis Avançats (ICREA) and Institut de Física d'Altes Energies (IFAE), Barcelona, Spain

³⁷Uppsala University, Uppsala, Sweden

³⁸Taras Shevchenko National University of Kyiv, Kiev, Ukraine

³⁹Lancaster University, Lancaster LA1 4YB, United Kingdom

⁴⁰Imperial College London, London SW7 2AZ, United Kingdom

⁴¹The University of Manchester, Manchester M13 9PL, United Kingdom

⁴²University of Arizona, Tucson, Arizona 85721, USA

⁴³University of California Riverside, Riverside, California 92521, USA

⁴⁴Florida State University, Tallahassee, Florida 32306, USA

⁴⁵Fermi National Accelerator Laboratory, Batavia, Illinois 60510, USA

⁴⁶University of Illinois at Chicago, Chicago, Illinois 60607, USA

⁴⁷Northern Illinois University, DeKalb, Illinois 60115, USA

⁴⁸Northwestern University, Evanston, Illinois 60208, USA

⁴⁹Indiana University, Bloomington, Indiana 47405, USA

⁵⁰Purdue University Calumet, Hammond, Indiana 46323, USA

⁵¹University of Notre Dame, Notre Dame, Indiana 46556, USA

⁵²Iowa State University, Ames, Iowa 50011, USA

⁵³University of Kansas, Lawrence, Kansas 66045, USA

⁵⁴Louisiana Tech University, Ruston, Louisiana 71272, USA

⁵⁵Northeastern University, Boston, Massachusetts 02115, USA

⁵⁶University of Michigan, Ann Arbor, Michigan 48109, USA

⁵⁷Michigan State University, East Lansing, Michigan 48824, USA

⁵⁸University of Mississippi, University, Mississippi 38677, USA

- ⁵⁹University of Nebraska, Lincoln, Nebraska 68588, USA
⁶⁰Rutgers University, Piscataway, New Jersey 08855, USA
⁶¹Princeton University, Princeton, New Jersey 08544, USA
⁶²State University of New York, Buffalo, New York 14260, USA
⁶³University of Rochester, Rochester, New York 14627, USA
⁶⁴State University of New York, Stony Brook, New York 11794, USA
⁶⁵Brookhaven National Laboratory, Upton, New York 11973, USA
⁶⁶Langston University, Langston, Oklahoma 73050, USA
⁶⁷University of Oklahoma, Norman, Oklahoma 73019, USA
⁶⁸Oklahoma State University, Stillwater, Oklahoma 74078, USA
⁶⁹Brown University, Providence, Rhode Island 02912, USA
⁷⁰University of Texas, Arlington, Texas 76019, USA
⁷¹Southern Methodist University, Dallas, Texas 75275, USA
⁷²Rice University, Houston, Texas 77005, USA
⁷³University of Virginia, Charlottesville, Virginia 22904, USA
⁷⁴University of Washington, Seattle, Washington 98195, USA
(Dated: August 21, 2014)

We present a measurement of the fundamental parameter of the standard model, the weak mixing angle $\sin^2 \theta_{\text{eff}}^\ell$ which determines the relative strength of weak and electromagnetic interactions, in $p\bar{p} \rightarrow Z/\gamma^* \rightarrow e^+e^-$ events at a center of mass energy of 1.96 TeV, using data corresponding to 9.7 fb⁻¹ of integrated luminosity collected by the D0 detector at the Fermilab Tevatron. The effective weak mixing angle is extracted from the forward-backward charge asymmetry as a function of the invariant mass around the Z boson pole. The measured value of $\sin^2 \theta_{\text{eff}}^\ell = 0.23147 \pm 0.00047$ is the most precise measurement from light quark interactions to date, with a precision close to the best LEP and SLD results.

PACS numbers: 12.15.-y, 12.15.Mm, 13.85.Qk, 14.70.Hp

The weak mixing angle $\sin^2 \theta_W$ is one of the fundamental parameters of the standard model (SM). It describes the relative strength of the axial-vector couplings g_A^f to the vector couplings g_V^f in neutral-current interactions of a Z boson to fermions f with Lagrangian

$$\mathcal{L} = -i \frac{g}{2 \cos \theta_W} \bar{f} \gamma^\mu \left(g_V^f - g_A^f \gamma_5 \right) f Z_\mu, \quad (1)$$

with $g_V^f = I_3^f - 2Q_f \cdot \sin^2 \theta_W$, $g_A^f = I_3^f$, where I_3^f and Q_f are the weak isospin component and the charge of the fermion. At tree level and in all orders of the on-shell renormalization scheme, the weak mixing angle can be written in terms of the W and Z boson masses as $\sin^2 \theta_W = 1 - M_W^2/M_Z^2$. To include higher order electroweak radiative corrections, effective weak mixing an-

gles are defined as

$$\sin^2 \theta_{\text{eff}}^f = \frac{1}{4|Q_f|} \left(1 - \frac{g_V^f}{g_A^f} \right), \quad (2)$$

for each fermion flavor.

It is customary to quote the charged lepton effective weak mixing angle $\sin^2 \theta_{\text{eff}}^\ell$, determined by measurements of observables around the Z boson pole. There is tension between the two most precise measurements of $\sin^2 \theta_{\text{eff}}^\ell$, which are 0.23221 ± 0.00029 from the combined LEP measurement using the charge asymmetry $A_{FB}^{0,b}$ for b quark production and 0.23098 ± 0.00026 from the SLD measurement of the e^+e^- left-right polarization asymmetry A_{lr} [1]. An independent determination of the effective weak mixing angle is therefore an important precision test of the SM electroweak breaking mechanism.

At the Tevatron, the mixing angle can be measured in the Drell-Yan process $p\bar{p} \rightarrow Z/\gamma^* \rightarrow \ell^+\ell^-$, through a forward-backward charge asymmetry in the distribution of the emission angle θ^* of the negatively charged lepton momentum relative to the incoming quark momentum, defined in the Collins-Soper frame [2]. Events with $\cos \theta^* > 0$ are classified as forward (F), and those with $\cos \theta^* < 0$ as backward (B). The forward-backward charge asymmetry, A_{FB} , is defined by

$$A_{FB} = \frac{N_F - N_B}{N_F + N_B}, \quad (3)$$

where N_F and N_B are the numbers of forward and backward events. The asymmetry arises from the interference

*with visitors from ^aAugustana College, Sioux Falls, SD, USA, ^bThe University of Liverpool, Liverpool, UK, ^cDESY, Hamburg, Germany, ^dUniversidad Michoacana de San Nicolas de Hidalgo, Morelia, Mexico ^eSLAC, Menlo Park, CA, USA, ^fUniversity College London, London, UK, ^gCentro de Investigacion en Computacion - IPN, Mexico City, Mexico, ^hUniversidade Estadual Paulista, São Paulo, Brazil, ⁱKarlsruher Institut für Technologie (KIT) - Steinbuch Centre for Computing (SCC), D-76128 Karlsruhe, Germany, ^jOffice of Science, U.S. Department of Energy, Washington, D.C. 20585, USA, ^kAmerican Association for the Advancement of Science, Washington, D.C. 20005, USA, ^lKiev Institute for Nuclear Research, Kiev, Ukraine, ^mUniversity of Maryland, College Park, Maryland 20742, USA and ⁿEuropean Organization for Nuclear Research (CERN), Geneva, Switzerland

between vector and axial vector coupling terms.

The asymmetry A_{FB} can be measured as a function of the invariant mass of the dilepton pair (M_{ee}). The presence of both vector and axial-vector couplings of the Z boson to fermions gives the most significant variation of A_{FB} in vicinity of the Z boson pole, which is sensitive to the effective weak mixing angle.

Measurements of $\sin^2 \theta_{\text{eff}}^\ell$ have been reported previously by the CDF Collaboration in the $Z \rightarrow e^+e^-$ [3, 4] and $Z \rightarrow \mu^+\mu^-$ [5] channels, and the D0 Collaboration in the $Z \rightarrow e^+e^-$ channel [6, 7]. The angle $\sin^2 \theta_{\text{eff}}^\ell$ has also been measured at the LHC in pp collisions by the CMS Collaboration in the $Z \rightarrow \mu^+\mu^-$ channel at $\sqrt{s} = 7$ TeV [8].

This letter reports a measurement of the effective weak mixing angle from the A_{FB} distribution using 9.7 fb^{-1} of integrated luminosity collected with the D0 detector at the Fermilab Tevatron collider. The precision of the previous D0 measurement using 5 fb^{-1} of data [7], $\sin^2 \theta_{\text{eff}}^\ell = 0.2309 \pm 0.0008$ (stat.) ± 0.0006 (syst.), was dominated by the statistical uncertainty and the uncertainty on the electron energy scale. The analysis of the full 9.7 fb^{-1} data set presented here features an extended acceptance and a new electron energy calibration method providing substantially improved accuracy.

The D0 detector comprises a central tracking system, a calorimeter and a muon system [9–11]. The central tracking system consists of a silicon microstrip tracker and a scintillating central fiber tracker, both located within a 1.9 T superconducting solenoidal magnet and optimized for tracking and vertexing capabilities at detector pseudorapidities of $|\eta_{\text{det}}| < 3$ [12]. Outside the solenoid, three liquid argon and uranium calorimeters provide coverage of $|\eta_{\text{det}}| < 3.5$ for electrons: the central calorimeter (CC) for $|\eta_{\text{det}}| < 1.1$, and two endcap calorimeters (EC) in the range $1.5 < |\eta_{\text{det}}| < 3.5$. Gaps between the cryostats create inefficient electron detection regions between $1.1 < |\eta_{\text{det}}| < 1.5$ that are excluded from the analysis. The muon system outside the calorimeter consists of drift chambers and scintillators before and after iron toroid magnets. The solenoid and toroid polarities are reversed every two weeks on average.

The data used in this analysis are collected by triggers requiring at least two electromagnetic (EM) clusters reconstructed in the calorimeter. The determination of their energies uses only the calorimeter information. Each EM cluster is further required to be in the CC or EC, with transverse momentum $p_T > 25$ GeV, and to have shower shapes consistent with that of an electron. For events with both EM candidates in the CC region (CC-CC), each EM object must have a spatially matched track reconstructed in the tracking system. For events with one EM cluster in the CC and the other in the EC region (CC-EC), only the CC candidate is required to have a matched track. For events with both candidates in the EC calorimeter (EC-EC), at least one EM object must have a matched track. All tracks must

have $p_T > 10$ GeV and satisfy track quality criteria to maintain a low charge mis-identification probability. For CC-CC events, the two EM candidates are required to have opposite charges. For CC-EC events, the determination of “forward” or “backward” is made according to the charge measured for the track-matched CC EM candidate, whereas the charge of the EC higher quality matched track is used for EC-EC events [13].

Events are further required to have a reconstructed dielectron invariant mass in the range $75 < M_{ee} < 115$ GeV. A larger sample satisfying $60 < M_{ee} < 130$ GeV is used to understand detector responses and to tune the Monte Carlo (MC) simulation.

To maximize the acceptance, previously ignored electrons reconstructed near the boundaries of CC calorimeter modules [9] (ϕ -mod boundary) are included. The geometric acceptance is further extended compared with previous D0 results [7] from $|\eta_{\text{det}}| < 1.0$ to $|\eta_{\text{det}}| < 1.1$ for the CC, and from $1.5 < |\eta_{\text{det}}| < 2.5$ to $1.5 < |\eta_{\text{det}}| < 3.2$ for the EC. In addition, EC-EC events, which were excluded due to their poorer track reconstruction and calorimeter energy resolution, are now included. The extensions in η_{det} and ϕ -mod acceptance give a 70% increase in the number of events over what would be expected from the increase in integrated luminosity. An additional 15% increase is gained from improvements in the track reconstruction algorithm. The number of $Z \rightarrow e^+e^-$ candidate events in the data sample is 560,267 which includes 248,380 CC-CC events, 240,593 CC-EC events and 71,294 EC-EC events.

The MC Drell-Yan $Z/\gamma^* \rightarrow e^+e^-$ sample is generated by using the D0 simulation software, based on the leading-order PYTHIA generator [14] with the NNPDF2.3 [15] parton distribution functions (PDFs), followed by a GEANT-based simulation [16] of the D0 detector. The PYTHIA MC samples, with data events from random beam crossings overlaid, are mainly used to understand the geometric acceptance, and the energy scale and resolution of electrons in the calorimeter.

A new method of electron energy calibration is developed and applied to both the data and MC, which significantly reduces the systematic uncertainty due to the electron energy measurement. The weak mixing angle, which is extracted from A_{FB} as a function of M_{ee} , depends strongly on the position of the peak value of M_{ee} . Therefore, it is critical to have a precise electron energy measurement and a consistent measured peak value of M_{ee} from different regions of the detector across various Tevatron running conditions. In Ref. [7], an overall scale factor was applied to simulations to model the detector response for electron energy depositions, where the scale factor is determined by comparing the M_{ee} spectrum in data and MC, yielding a large uncertainty due to background estimation and detector resolution. In this analysis, a new energy calibration method is applied to the data and the MC separately. The energy mea-

surement depends not only on the η_{det} , but also on the instantaneous luminosity [17]. For CC electrons, an instantaneous luminosity-dependent scale factor (α_L^{CC}) and an η_{det} -dependent scale factor (α_η^{CC}) are applied to the electron energy. For EC electrons in addition to the scale factors α_L^{EC} and α_η^{EC} , an η_{det} -dependent offset β_η^{EC} is introduced to model the η_{det} dependence of the electron energy. All correction factors are determined by scaling the peak of the M_{ee} distribution as a function of instantaneous luminosity and η_{det} to be consistent with the Z boson mass measured by LEP ($M_Z = 91.1875$ GeV) [1]. The CC correction factors are tuned with the CC-CC events. To remove one degree of freedom, β_η^{EC} is expressed as a function of α_η^{EC} , and the relationship is measured with the CC-EC events. The values of α_η^{EC} and $\beta_\eta^{\text{EC}}(\alpha_\eta^{\text{EC}})$ are fitted using the EC-EC events. After the calibration, the standard deviation δM of the M_{ee} peak values in different η_{det} regions is ≈ 20 MeV. Various closure tests are performed to check the validity of the calibration procedure. For example, an extra η_{det} -dependent offset is applied to the corrected energy and fixed by performing the calibration again. The extra offset is found to be consistent with δM . The ratio of δM to M_Z is propagated into the uncertainty of the $\sin^2 \theta_{\text{eff}}^\ell$ measurement to estimate the systematic uncertainty arising from the energy calibration.

After the electron energy calibration, an additional electron energy resolution smearing is derived and applied to the MC to achieve agreement with the width of the M_{ee} distribution in data. For the CC ϕ -mod boundary electrons, the resolution smearing is modeled with a Crystal Ball function [18]. For other electrons, the smearing is modeled with a Gaussian function.

Additional corrections and reweightings are applied to the MC simulation to improve the agreement with data. The scale factors of the electron identification efficiency between the MC and the data are measured using the tag-and-probe method [19] and applied to the MC distributions as functions of p_T and η_{det} . The simulation is further corrected for higher-order effects not included in PYTHIA by reweighting the MC events at the generator level in two dimensions (p_T and rapidity y of the Z boson) to match RESBOS [20] predictions. In addition, next-to-next-to-leading order QCD corrections are applied as a function of M_Z [20, 21]. The distribution of the instantaneous luminosity and the z coordinate of the $p\bar{p}$ collision vertices are also weighted to match those in the data. Since A_{FB} is defined as a ratio of numbers of events, many small uncertainties cancel out. Only the electron selection efficiency scale factor in these additional corrections contributes significantly to the final uncertainty.

The charge of the particle track matched to the EM cluster is used to determine if the EM cluster is associated to an electron or positron and to classify the event as forward or backward. The charge misidentification prob-

ability is given by the number of $p\bar{p} \rightarrow Z/\gamma^* \rightarrow e^+e^-$ events reconstructed with same-sign as a proportion of the total number of $p\bar{p} \rightarrow Z/\gamma^* \rightarrow e^+e^-$ events. The probabilities are measured in data and MC. The charge of electrons and positrons reconstructed in the MC is randomly changed to match the misidentification probability in the data averaged over p_T spectrum of electrons. In the CC region the average charge misidentification rate in data is about 0.3%, whereas in the EC region it varies from 1% at $|\eta_{\text{det}}| = 1.5$ to 10% at $|\eta_{\text{det}}| = 3.0$. The statistical uncertainty of the measured charge misidentification rate is included as a systematic uncertainty.

The background is suppressed by the strict requirements on the quality of the matched track. The main contribution is from multijet events, in which jets are misreconstructed as electrons, and is estimated from data. The multijet production from the proton anti-proton initial state produces jets, and hence fake electrons, nearly symmetrically with respect to the forward and backward hemispheres [7, 22]. Multijet events are selected by reversing some of the electron selection cuts to study the differential distributions of the multijet background, which are different from the real multijet background that passes all the electron selections. Therefore, a correction factor is applied as a function of electron p_T , given by the ratios of the efficiencies for EM-like jets (which are selected in a multijet-enriched data sample and pass all the electron selections) and ‘‘reverse-selected’’ jets. The normalization of the multijet background is determined by fitting the sum of the M_{ee} distributions of multijet events and the signal MC events to the distribution from the selected data events. The W +jets, $Z/\gamma^* \rightarrow \tau\tau$, diboson (WW and WZ), $\gamma\gamma$ and $t\bar{t}$ backgrounds are estimated using the PYTHIA MC simulations. At the Z boson peak, the multijet background is 0.3% and the sum of the di-boson, W +jets, $Z/\gamma^* \rightarrow \tau\tau$, $\gamma\gamma$ and $t\bar{t}$ backgrounds is about 0.05%. The M_{ee} and $\cos\theta^*$ distributions of data and of the sum of signal MC and background expectations are in good agreement with the SM predictions [23].

The AFB distributions as a function of mass are obtained for CC-CC, CC-EC and EC-EC categories by summing the samples of specific solenoid and toroid magnet polarities, after weighting each by the integrated luminosity for the sample. This weighted combination provides cancellation of asymmetries due to variations in detector response and acceptance with η_{det} and p_T . The weak mixing angle is extracted from the background-subtracted A_{FB} spectrum in the regions $75 < M_{ee} < 115$ GeV for CC-CC and CC-EC events, and $81 < M_{ee} < 97$ GeV for EC-EC events by comparing the data to simulated A_{FB} templates corresponding to different input values of $\sin^2 \theta_W$. The mass window for EC-EC events is narrower to take into account the differences in track reconstruction and energy measurement. The templates are obtained by reweighting M_Z and $\cos\theta^*$ distributions at the generator level to different Born-level $\sin^2 \theta_W$ pre-

	CC-CC	CC-EC	EC-EC	Combined
$\sin^2 \theta_W$	0.23142	0.23143	0.22977	0.23139
Statistical	0.00116	0.00047	0.00276	0.00043
Systematic	0.00009	0.00009	0.00019	0.00008
Energy Calibration	0.00003	0.00001	0.00004	0.00001
Energy Smearing	0.00001	0.00002	0.00013	0.00002
Background	0.00002	0.00001	0.00002	0.00001
Charge Misidentification	0.00002	0.00004	0.00012	0.00003
Electron Identification	0.00008	0.00008	0.00005	0.00007
Fiducial Asymmetry	0.00002	0.00001	0.00001	0.00001
Total	0.00116	0.00048	0.00277	0.00044

TABLE I: Measured $\sin^2 \theta_W$ values and corresponding uncertainties. Uncertainties from higher-order corrections and the PDFs are not included.

distributions. The A_{FB} distribution is negligibly sensitive to the effect of QED final state radiation because most of these radiated photons are emitted co-linearly with the electron and are reconstructed as one single EM object by the detector. The background-subtracted A_{FB} distribution and the PYTHIA prediction with the fitted $\sin^2 \theta_W$ are shown in Fig. 1.

The results of the fits for different event categories, with statistical and systematic uncertainties, are listed in Table I. The uncertainties on $\sin^2 \theta_W$ are dominated by the limited data sample. CC-EC events are the most sensitive to the weak mixing angle due to the larger variation of A_{FB} with mass in that kinematic region. The systematic uncertainties due to the electron energy calibration and resolution smearing, the estimation of the backgrounds, the charge misidentification rate and the identification efficiency are also dominated by the limited data sample. We estimate the systematic uncertainty on the measured $\sin^2 \theta_W$ due to instrumental asymmetries that remain after combining the luminosity-weighted solenoid and toroid samples to be ± 0.00001 .

The measurement is dominated by statistical uncertainties. Systematic uncertainties are treated as uncorrelated but the total uncertainty does not depend on whether they are taken to be correlated or uncorrelated. The results were therefore combined by using the corresponding uncertainties as weights, giving

$$\begin{aligned} \sin^2 \theta_W = & \\ & 0.23139 \pm 0.00043 \text{ (stat.)} \pm \\ & 0.00008 \text{ (syst.)} \pm 0.00017 \text{ (PDF)}. \end{aligned}$$

The PDF uncertainty is estimated by reweighting the PDF set in the MC simulations to different sets of the NNPDF2.3, computing the $\sin^2 \theta_W$ value for each set, and taking the standard deviation of these values as the uncertainty [15].

To have a consistent SM definition and make our result comparable with previous measurements, a LO PYTHIA interpretation of the weak mixing angle with CTEQ6.6

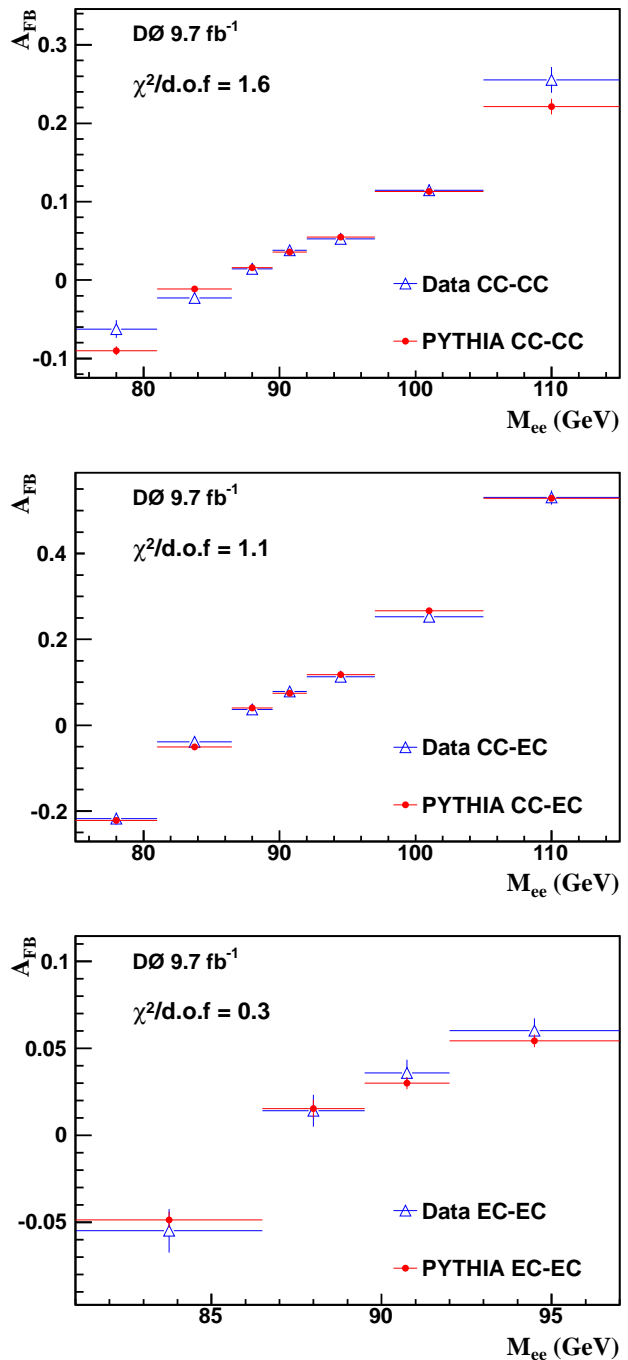


FIG. 1: (color online). Comparison between the A_{FB} distributions measured in the background-subtracted data and the MC for the three kinematic regions, with the corresponding χ^2 per degree of freedom. $\sin^2 \theta_W$ in the MC is 0.23139. The error bars are statistical only.

PDF set [24] is compared to the predictions from a modified NLO RESBOS with the same PDF set. RESBOS has a more sophisticated treatment of electroweak effects and uses different values of effective weak mixing angle for

leptons and up or down quarks [25]. This study indicates that a 0.00008 positive shift in $\sin^2 \theta_W$ for RESBOS relative to LO PYTHIA that changes the measured leptonic effective weak mixing angle to $\sin^2 \theta_{\text{eff}}^\ell = 0.23147 \pm 0.00047$, with the same breakdown of uncertainties as above. The comparison between our measurement and other experimental results is shown in Fig. 2. Our measurement is consistent with the current world average.

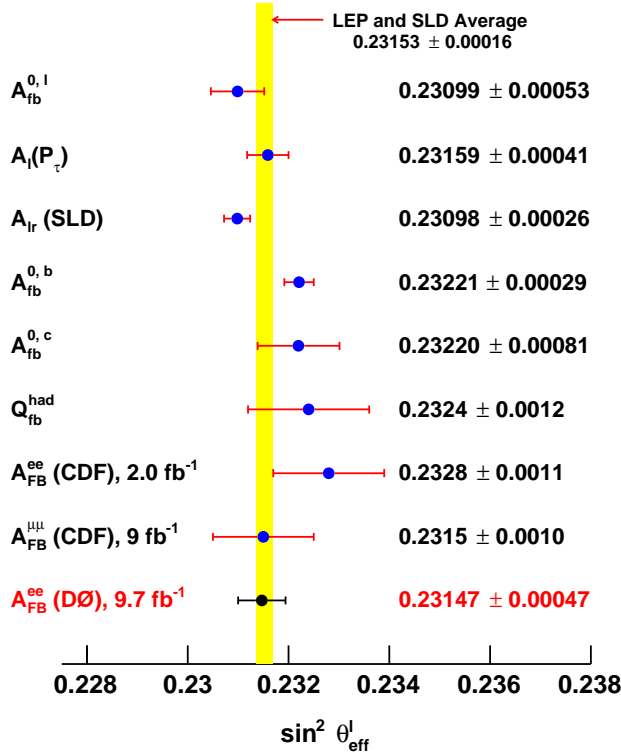


FIG. 2: (color online). Comparison of measured $\sin^2 \theta_{\text{eff}}^\ell$ with results from other experiments. The average is a combination of $A_{\text{FB}}^{0,\ell}$, $A_l(P_\tau)$, $A_{lr}(\text{SLD})$, $A_{\text{FB}}^{0,b}$, $A_{\text{FB}}^{0,c}$, and $Q_{\text{FB}}^{\text{had}}$ measurements from the LEP and SLD Collaborations [1].

In conclusion, we have measured the effective weak mixing angle $\sin^2 \theta_{\text{eff}}^\ell$ from the distribution of the forward-backward charge asymmetry A_{FB} in the process $p\bar{p} \rightarrow Z/\gamma^* \rightarrow e^+e^-$ at the Tevatron. This measurement, which supersedes that reported in [7], uses nearly twice the integrated luminosity and significantly extends the electron acceptance. The primary systematic uncertainty is reduced by introducing a new electron energy calibration method. The result from 9.7 fb^{-1} of integrated luminosity is $\sin^2 \theta_{\text{eff}}^\ell = 0.23147 \pm 0.00047$. This result is the most precise measurement from light quark interactions, and is close to the precision of the world's best measurements performed by the LEP and SLD Collaborations.

ACKNOWLEDGEMENTS

We thank the staffs at Fermilab and collaborating institutions, and acknowledge support from the Department of Energy and National Science Foundation (United States of America); Alternative Energies and Atomic Energy Commission and National Center for Scientific Research/National Institute of Nuclear and Particle Physics (France); Ministry of Education and Science of the Russian Federation, National Research Center ‘‘Kurchatov Institute’’ of the Russian Federation, and Russian Foundation for Basic Research (Russia); National Council for the Development of Science and Technology and Carlos Chagas Filho Foundation for the Support of Research in the State of Rio de Janeiro (Brazil); Department of Atomic Energy and Department of Science and Technology (India); Administrative Department of Science, Technology and Innovation (Colombia); National Council of Science and Technology (Mexico); National Research Foundation of Korea (Korea); Foundation for Fundamental Research on Matter (The Netherlands); Science and Technology Facilities Council and The Royal Society (United Kingdom); Ministry of Education, Youth and Sports (Czech Republic); Bundesministerium für Bildung und Forschung (Federal Ministry of Education and Research) and Deutsche Forschungsgemeinschaft (German Research Foundation) (Germany); Science Foundation Ireland (Ireland); Swedish Research Council (Sweden); China Academy of Sciences and National Natural Science Foundation of China (China); and Ministry of Education and Science of Ukraine (Ukraine).

- [1] G. Abbiendi *et al.* (LEP Collaborations ALEPH, DELPHI, L3 and OPAL, SLD Collaboration, LEP Electron-weak Working Group, SLD Electroweak, and Heavy Flavor Groups), *Phys. Rep.* **427**, 257 (2006).
- [2] J. C. Collins and D. E. Soper, *Phys. Rev. D* **16**, 2219 (1977).
- [3] D. Acosta *et al.* (CDF Collaboration), *Phys. Rev. D* **71**, 052002 (2005).
- [4] T. Aaltonen *et al.* (CDF Collaboration), *Phys. Rev. D* **88**, 072002 (2013).
- [5] T. Aaltonen *et al.* (CDF Collaboration), *Phys. Rev. D* **89**, 072005 (2014).
- [6] V. M. Abazov *et al.* (D0 Collaboration), *Phys. Rev. Lett.* **101**, 191801 (2008).
- [7] V. M. Abazov *et al.* (D0 Collaboration), *Phys. Rev. D* **84**, 012007 (2011).
- [8] S. Chatrchyan *et al.* (CMS Collaboration), *Phys. Rev. D* **84**, 112002 (2011).
- [9] V. M. Abazov *et al.* (D0 Collaboration), *Nucl. Instrum. Methods Phys. Res. A* **565**, 463 (2006).
- [10] M. Abolins *et al.* (D0 Collaboration), *Nucl. Instrum. Methods Phys. Res. A* **584**, 75 (2008).
- [11] R. Angstadt *et al.* (D0 Collaboration), *Nucl. Instrum.*

- Methods Phys. Res. A **622**, 298 (2010).
- [12] D0 uses a cylindrical coordinate system with the z axis along the beam axis in the proton direction. Angles θ and ϕ are the polar and azimuthal angles, respectively. Pseudorapidity is defined as $\eta = -\ln[\tan(\theta/2)]$ where θ is measured with respect to the interaction vertex. In the massless limit, η is equivalent to the rapidity $y = (1/2)\ln[(E+p_z)/(E-p_z)]$, and η_{det} is the pseudorapidity measured with respect to the center of the detector.
- [13] V. M. Abazov *et al.* (D0 Collaboration), Nucl. Instrum. Meth. A **750**, 78 (2014).
- [14] T. Sjöstrand, P. Edén, C. Feriberg, L. Lönnblad, G. Miu, S. Mrenna, and E. Norrbin, Comp. Phys. Commun. **135**, 238 (2001). PYTHIA version v6.323 is used throughout.
- [15] R. D. Ball *et al.*, Nucl. Phys. **B867**, 244 (2013).
- [16] R. Brun and F. Carminati, CERN Program Library Long Writeup W5013, 1993 (unpublished).
- [17] V. M. Abazov *et al.* (D0 Collaboration), Phys. Rev. D **89**, 012005 (2014).
- [18] J. E. Gaiser, Ph.D. Thesis, SLAC-R-255 (1982).
- [19] V. M. Abazov *et al.* (D0 Collaboration), Phys. Rev. D **76**, 012003 (2007).
- [20] C. Balazs and C. P. Yuan, Phys. Rev. D **56**, 5558 (1997).
- [21] R. Hamberg, W.L. van Neerven, and T. Matsuura, Nucl. Phys. **B359**, 343 (1991); R. Hamberg, W.L. van Neerven, and T. Matsuura, Nucl. Phys. **B644**, 430(E) (2002).
- [22] V. M. Abazov *et al.* (D0 Collaboration), Phys. Rev. D **88**, 112002 (2013).
- [23] See Supplemental Material at [temporary <http://www-d0.fnal.gov/Run2Physics/WWW/results/final/EW/E14> final link to be set by the editor] for additional plots supporting the analysis.
- [24] P. M. Nadolsky, H. -L. Lai, Q. -H. Cao, J. Huston, J. Pumplin, D. Stump, W. -K Tung and C. -P. Yuan, Phys. Rev. D **78**, 013004 (2008).
- [25] U. Baur, O. Brein, W. Hollik, C. Schappacher, and D. Wackerroth, Phys. Rev. D **65**, 033007, 2002